Excitations and quantum fluctuations in site-diluted two-dimensional antiferromagnets

Eduardo R. Mucciolo,[1] A. H. Castro Neto,[2] and Claudio Chamon[2]
[1]*Department of Physics, University of Central Florida, Orlando, Florida 32816, USA;*
Department of Physics, Duke University, Durham, North Carolina 27708, USA;
Departamento de Física, Pontifícia Universidade Católica do Rio de Janeiro, Caixa Postal 37801, 22452-970 Rio de Janeiro, Brazil
[2]*Department of Physics, Boston University, Boston, Massachusetts 02215, USA*
(Received 3 February 2004; published 24 June 2004)

We study the effect of site dilution and quantum fluctuations in an antiferromagnetic spin system on a square lattice within the linear spin-wave approximation. By performing numerical diagonalization in real space and finite-size scaling, we characterize the nature of the low-energy spin excitations for different dilution fractions up to the classical percolation threshold. We find nontrivial signatures of fractonlike excitations at high frequencies. Our simulations also confirm the existence of an upper bound for the amount of quantum fluctuations in the ground state of the system, leading to the persistence of long-range order up to the percolation threshold. This result is in agreement with recent neutron-scattering experimental data and quantum Monte Carlo numerical calculations. We also show that the absence of a quantum critical point below the classical percolation threshold holds for a large class of systems whose Hamiltonians can be mapped onto a system of coupled noninteracting massless bosons.

DOI: 10.1103/PhysRevB.69.214424 PACS number(s): 75.10.Jm, 75.50.Ee, 75.30.Ds, 75.40.Mg

I. INTRODUCTION

The problem of the interplay of quantum fluctuations and disorder in low dimensional systems is of fundamental importance in modern condensed matter physics. It is relevant for the understanding of the metal-insulator transition in metal-oxide-semiconductor field-effect transistors (MOSFETS),[1] impurity effects in *d*-wave superconductors,[2] non-Fermi-liquid behavior in U and Ce intermetallics,[3] and the persistence of long-range order (LRO) in two-dimensional (2D) spin-1/2 quantum antiferromagnets (AFM),[4] among others.

The 2D square lattice with nearest-neighbor hopping undergoes a classical percolation transition upon random dilution. For the case of site dilution, the transition occurs at the hole concentration $x_c \approx 0.41$,[5] while for bond dilution the largest (infinite) connected cluster disappears when exactly half of the bonds are absent (i.e., $x_c = 1/2$).[6,7] Thus, no ground-state long-range order is possible for any model with short-range interactions in these lattices above x_c. For those models where order does exist in the clean limit, it is natural to ask whether dilution can enhance quantum fluctuations to the point of destroying long-range order at some doping fraction below x_c. This possibility has led to several theoretical and experimental investigations in a variety of systems.[4,8–11] In particular, a recent neutron scattering experiment[4] in the site-diluted $S=1/2$ Heisenberg quantum AFM $La_2Cu_{1-x}(Zn,Mg)_xO_4$ (LCMO), indicates that LRO exists up to x_c. This fact was corroborated by an extensive quantum Monte Carlo (QMC) simulation[8] and by spin-wave theory (SWT) analytical calculation in the dilute regime.[9] The numerical and experimental data suggest that the disappearance of order in the ground state is dominated by a classical effect and no quantum phase transition takes place below x_c. The analytical calculation,[9] on the other hand, points to a nontrivial dilution-induced softening of low-frequency spin-wave excitations in determining the magnitude of quantum fluctuations. However, the latter was carried out within the *T*-matrix approximation, which excludes coherent superposition and interference, and thus could not account for strong localization effects.

In this work we carry out exact real space numerical diagonalizations of the dilute 2D Heisenberg AFM within the linear spin-wave approximation for dilution fractions ranging from the clean limit to the the classical percolation threshold. Although our method cannot be used to investigate systems as large as those used in previous numerical studies of the dynamical structure factor alone,[12] it provides complete access to eigenenergies and eigenvectors, thus allowing us to probe more carefully into the structure of the excited states of the site dilute AFM. We find that excitations in this system break up into different modes as the amount of dilution is increased. The multipeak structure of the spectral function shows the simultaneous existence of extended (magnons) and localized (fractons) excitations, similarly to what was observed experimentally by Uemura and Birgeneau for dilute *three-dimensional* AFMs several years ago.[13]

We also argue that the absence of a quantum critical point in diluted systems below x_c is a universal feature for a large class of continuous models of the Heisenberg type that can be mapped into a system of coupled harmonic oscillators within some approximate scheme. We establish an upper bound for the amount of quantum fluctuations in these diluted noninteracting bosonic systems and show that quantum fluctuations are bounded even at the percolation threshold for 2D systems. Indeed, one may wonder whether this generic behavior of diluted bosonic systems is related to universality classes dictated solely by symmetries of the disordered Hamiltonian, as in the case of fermionic models.

The paper is organized as follows. In Sec. II we define the system Hamiltonian and find the corresponding non-Hermitian eigenvalue matrix problem in lattice coordinates within the linear spin-wave approximation. In Sec. III we

present and discuss the numerical methods used to generate the random dilution, the identification of the largest connected cluster, and the diagonalization of the eigenvalue problem. The numerical results for the spin-wave excitation spectrum and the quantum fluctuation corrections to the AFM ground state are presented and discussed in Sec. IV. In Sec. V we argue that the absence of quantum phase transitions in site dilute systems occurs for spin Hamiltonians that can be mapped onto a system of coupled harmonic oscillators. Finally, in Sec. VI, we draw our conclusions and point to future directions.

II. DILUTE HEISENBERG ANTIFERROMAGNET IN THE SPIN-WAVE APPROXIMATION

We begin by reviewing the well-known connection between magnetic and bosonic systems. In particular, we are interested in spin Hamiltonians of the form

$$H = \sum_{\langle i,j\rangle,a} \eta_i \eta_j J_a S_i^a S_j^a, \tag{1}$$

where S_i^a is the $a=x,y,z$ component of a spin S at site i, J_a is the nearest-neighbor exchange constant, and $\eta_i=0(1)$ if the site is empty (occupied). The empty sites are randomly distributed over the whole sample with uniform probability. Calling N the total number of sites, we define the fraction of occupied sites as

$$p = \frac{1}{N}\sum_{i=1}^{N} \eta_i. \tag{2}$$

The dilution fraction is then defined as $x=1-p$.

The isotropic AFM Heisenberg model corresponds to $J_a = J>0$ for $a=x,y,z$. When LRO is present (say, along the z direction), the spin operators can be written in terms of bosonic operators using the Holstein-Primakoff method.[14] Since the square lattice is bipartite, it can be divided up into two square sublattices, $\mathcal{A}=\mathcal{L}_+$ and $\mathcal{B}=\mathcal{L}_-$. Thus,

$$S_{i\,z} = S - a_i^\dagger a_i, \tag{3}$$

$$S_i^+ = [2S - a_i^\dagger a_i]^{1/2} a_i, \tag{4}$$

$$S_i^- = a_i^\dagger [2S - a_i^\dagger a_i]^{1/2}, \tag{5}$$

with $i \in \mathcal{A}$, and

$$S_{j\,z} = -S + b_j^\dagger b_j, \tag{6}$$

$$S_j^+ = b_j^\dagger [2S - b_j^\dagger b_j]^{1/2}, \tag{7}$$

$$S_j^- = [2S - b_j^\dagger b_j]^{1/2} b_j, \tag{8}$$

with $j \in \mathcal{B}$. The bosonic operators obey the usual commutation relations, namely,

$$[a_i, a_{i'}^\dagger] = \delta_{ii'} \quad \text{and} \quad [b_j, b_{j'}^\dagger] = \delta_{jj'}, \tag{9}$$

with all other commutators equal to zero.

For the large spin case ($S \gg 1$) or when the number of spin waves is small ($n_i=\langle a_i\, a_i^\dagger\rangle$, $n_j=\langle b_j\, b_j^\dagger\rangle \ll S$), we can expand the square root in Eqs. (3) and (6) in powers of n_i and n_j, keeping only linear terms. That allows us to write the approximate bilinear bosonic Hamiltonian

$$H \approx -JS^2 \sum_{\langle ij\rangle} \eta_i \eta_j + JS \sum_{\langle ij\rangle} \eta_i \eta_j (a_i^\dagger a_i + b_j^\dagger b_j + a_i b_j + a_i^\dagger b_j^\dagger). \tag{10}$$

The first term on the right-hand side of Eq. (10) represents the classical ground-state energy of the AFM. Using the bosonic commutation relations, we can rearrange the Hamiltonian in the following form:

$$H \approx -JS(S+1) \sum_{\langle ij\rangle} \eta_i \eta_j + H_{\mathrm{SW}}, \tag{11}$$

where, now, the first term on the right-hand side represents the ground-state energy in the absence of quantum fluctuations, while the latter is described by the second term,

$$H_{\mathrm{SW}} = \frac{JS}{2} \sum_{\langle ij\rangle} \eta_i \eta_j (a_i^\dagger a_i + a_i a_i^\dagger + b_j^\dagger b_j + b_j b_j^\dagger + a_i b_j + b_j a_i + a_i^\dagger b_j^\dagger + b_j^\dagger a_i^\dagger). \tag{12}$$

Hereafter we will drop the constant ground-state energy term and will only study the eigenstates of H_{SW}. The spin-wave Hamiltonian contains bilinear crossed terms which, separately, do not conserve particle number. At this point, it is worth simplifying the notation by dropping the distinction between bosonic operators living on different sublattices and reordering the summation over sites,

$$H_{\mathrm{SW}} = \frac{JS}{2} \sum_{i,j=1}^{N} [K_{ij}(a_i^\dagger a_j + a_i a_j^\dagger) + \Delta_{ij}(a_i a_j + a_i^\dagger a_j^\dagger)], \tag{13}$$

where both indexes in the sum run over all sites in the lattice. The matrices K and Δ are defined as

$$K_{ij} = \delta_{ij} \sum_{\langle il\rangle} \eta_l \tag{14}$$

(the sum run over all nearest-neighbor sites to i) and

$$\Delta_{ij} = \begin{cases} \eta_i \eta_j & \text{for } i,j \text{ nearest neighbors} \\ 0, & \text{otherwise.} \end{cases} \tag{15}$$

Notice that both matrices K and Δ are real and symmetric.

A. Bogoliubov transformation

It is possible to diagonalize the spin-wave Hamiltonian through an operator transformation of the Bogoliubov type,

$$a_i = \sum_n (u_{in}\, \alpha_n + v_{in}\, \alpha_n^\dagger), \tag{16}$$

$$a_i^\dagger = \sum_n (v_{in}^*\, \alpha_n + u_{in}^*\, \alpha_n^\dagger), \tag{17}$$

or, in matrix notation,

$$\begin{pmatrix} \overline{a} \\ \overline{a^*} \end{pmatrix} = \begin{pmatrix} U & V \\ V^* & U^* \end{pmatrix} \begin{pmatrix} \overline{\alpha} \\ \overline{\alpha^*} \end{pmatrix}, \tag{18}$$

where the column vectors $\overline{a}$ and $\overline{\alpha}$ contain the operators a_i and α_n, respectively, while the $N \times N$ matrices U and V contain the coefficients $\{u_{in}\}$ and $\{v_{in}\}$, respectively, with $i,n = 1, \ldots, N$. Assuming that the new operators also obey the canonical commutation relations,

$$[\alpha_n, \alpha_m^\dagger] = \delta_{nm} \quad \text{and} \quad [\alpha_n, \alpha_m] = [\alpha_n^\dagger, \alpha_m^\dagger] = 0, \tag{19}$$

one arrives at the following constraints for the transformation coefficients:

$$\sum_{n=1}^{N} (u_{in}^* u_{jn} - v_{in} v_{jn}^*) = \delta_{ij} \tag{20}$$

and

$$\sum_{n=1}^{N} (u_{in}\, v_{jn} - v_{in}\, u_{jn}) = 0. \tag{21}$$

In matrix notation,

$$U\, U^\dagger - V\, V^\dagger = I_N \tag{22}$$

and

$$U\, V^T - V\, U^T = 0, \tag{23}$$

where I_N is the $N \times N$ unit matrix. These relations can be put into a more compact form by defining the matrices

$$T = \begin{pmatrix} U & V \\ V^* & U^* \end{pmatrix} \tag{24}$$

and

$$\Sigma = \begin{pmatrix} I_N & 0 \\ 0 & -I_N \end{pmatrix}. \tag{25}$$

Thus, Eqs. (22) and (23) become one,

$$T\, \Sigma\, T^\dagger = \Sigma. \tag{26}$$

Since $\Sigma^2 = I_{2N}$, we find, after a simple algebra, that

$$T^\dagger \Sigma\, T = \Sigma. \tag{27}$$

As a result we have two additional (though not independent) sets of orthogonality equations,

$$\sum_{i=1}^{N} (u_{in}^*\, u_{im} - v_{in}\, v_{im}^*) = \delta_{nm} \tag{28}$$

and

$$\sum_{i=1}^{N} (u_{in}^*\, v_{im} - v_{in}\, u_{im}^*) = 0. \tag{29}$$

B. Non-Hermitian eigenvalue problem (Ref. 15)

The transformation defined by Eq. (18) allows us to diagonalize the spin-wave Hamiltonian in terms of the new bosonic operators. For that purpose, we choose T such that

$$T^\dagger \begin{pmatrix} K & \Delta \\ \Delta & K \end{pmatrix} T = \begin{pmatrix} \Omega_+ & 0 \\ 0 & \Omega_- \end{pmatrix}, \tag{30}$$

where $\Omega_\pm$ are diagonal matrices containing the eigenfrequencies: $[\Omega_\pm]_{nn} = \omega_n^{(\pm)}$ for $n = 1, \ldots, N$. The eigenvalue problem defined by Eq. (30) can be further simplified. Recalling Eq. (27), we have that

$$\begin{pmatrix} K & \Delta \\ \Delta & K \end{pmatrix} T = \Sigma\, T\, \Sigma \begin{pmatrix} \Omega_+ & 0 \\ 0 & \Omega_- \end{pmatrix}. \tag{31}$$

In fact, it is not difficult to prove that eigenfrequency matrices obey the relation $\Omega_+ = \Omega_-^* = \Omega$, with Ω being a diagonal matrix with real entries only, as one physically expects. As a result,

$$\begin{pmatrix} K & \Delta \\ \Delta & K \end{pmatrix} \begin{pmatrix} U & V \\ V^* & U^* \end{pmatrix} = \begin{pmatrix} U & -V \\ -V^* & U^* \end{pmatrix} \begin{pmatrix} \Omega & 0 \\ 0 & \Omega \end{pmatrix}. \tag{32}$$

We can break up this $2N \times 2N$ matrix equation into two coupled $N \times N$ matrix equations,

$$K\, U + \Delta\, V^* = U\, \Omega,$$

$$\Delta\, U + K\, V^* = -V^*\, \Omega, \tag{33}$$

or, alternatively, writing explicitly the matrix elements,

$$\sum_j [K_{ij}\, u_{jn} + \Delta_{ij}\, v_{jn}^*] = \omega_n\, u_{in}, \tag{34}$$

$$\sum_j [\Delta_{ij}\, u_{jn} + K_{ij}\, v_{jn}^*] = -\omega_n\, v_{in}^*, \tag{35}$$

for all n and i. Thus, for a given eigenstate n, we can define an eigenvalue matrix equation in the usual form, namely,

$$\begin{pmatrix} K & \Delta \\ -\Delta & -K \end{pmatrix} \begin{pmatrix} u_n \\ v_n^* \end{pmatrix} = \omega_n \begin{pmatrix} u_n \\ v_n^* \end{pmatrix}. \tag{36}$$

(Notice that each u_n and v_n is now a column vector with components running through all $i = 1, \ldots, N$ lattice sites.) The $2N \times 2N$ matrix shown in Eq. (36) is clearly non-Hermitian, but its eigenvalues are all real. Notice also that if ω_n is an eigenvalue with corresponding eigenvector (u_n, v_n^*), then $-\omega_n$ is also an eigenvalue, but with (v_n^*, u_n) as the corresponding eigenvector. Thus, despite the fact that the non-Hermitian matrix provides $2N$ eigenvalues (eigenfrequencies), we should only keep those N that are positive and whose corresponding coefficients u_{in} and v_{in} satisfy Eqs. (20), (21), (28), and (29).

The non-Hermitian matrix in Eq. (36) contains only integer elements: 0, 1, 2, or 4 in the diagonal (corresponding to K_{ii}, i.e., the number of nearest neighbors to site i) and 0 or 1 in the off-diagonal components (corresponding to Δ_{ij}, i.e., 1 when i and j are nearest neighbors and zero otherwise). It is strongly sparse, although without any particularly simple pattern due to the presence of dilution disorder.

It is easy to verify that there are at least two zero modes in Eq. (36), i.e., two distinct nontrivial solutions with zero eigenvalue:

$$u_{i0}^{(a)} = 1, \quad v_{i0}^{(a)} = -1, \tag{37}$$

for all $i=1,\ldots,N$, and

$$u_{i0}^{(b)} = v_{i0}^{(b)} = \begin{cases} 1, & i \in \mathcal{A}, \\ -1, & i \in \mathcal{B}. \end{cases} \tag{38}$$

(In order to prove that these are indeed eigenstates, notice that $\Sigma_{j=1}^{N} \Delta_{ij} = K_{ii}$.) These two zero modes do not obey the orthogonality relation of Eq. (28); they have zero hyperbolic norm instead.

C. Average magnetization per site

The total staggered magnetization can be written in terms of the expectation value of the spin-wave number operator:

$$M_z^{\text{stagg}} = \left\langle \sum_{i\in A} S_{i\,z} - \sum_{j\in B} S_{j\,z} \right\rangle = NS - \sum_{i=1}^{N} \langle a_i^\dagger a_i \rangle, \tag{39}$$

where we have assumed that the sublattices contain the same number of sites: $N_A = N_B = N/2$. As a result, the average staggered spin per site along the z direction can be written as

$$m_z = \frac{M_z^{\text{stagg}}}{N} = S - \delta m_z, \tag{40}$$

with

$$\delta m_z = \frac{1}{N} \sum_{i=1}^{N} \delta m_i^z, \tag{41}$$

and

$$\delta m_i^z = \langle a_i^\dagger a_i \rangle. \tag{42}$$

Notice that δm_z describes the spin-wave correction to the average staggered magnetization (always a reduction).

In order to express δm_z in terms of the coefficients v_{in} and u_{in}, we use Eqs. (16) and (17) to first write the site magnetization at zero temperature in terms of eigenmodes. Upon taking the ground-state expectation value, we have to recall that the vacuum contains zero eigenmodes. Hence,

$$\langle \alpha_n \alpha_m \rangle = \langle \alpha_n^\dagger \alpha_m^\dagger \rangle = \langle \alpha_n^\dagger \alpha_m \rangle = 0, \tag{43}$$

while

$$\langle \alpha_n \alpha_m^\dagger \rangle = \delta_{nm}. \tag{44}$$

As a result,

$$\delta m_i^z = \sum_{n=2}^{N} |v_{in}|^2, \tag{45}$$

where the sum runs only through eigenmodes with *positive* frequency (the zero modes have been subtracted).

D. Reduction to an $N\times N$ non-Hermitian eigenvalue problem

It is possible to rewrite the $2N\times 2N$ eigenvalue problem as two coupled eigenproblems, each one of order $N\times N$ instead. The non-Hermitian character of the matrices involved does not change. However, the amount of work for numerical computations decreases by a factor of 4 [recall that diagonalizing a $N\times N$ requires $O(N^3)$ operations].

We begin by summing and subtracting Eqs. (34) and (35), obtaining

$$\sum_{j=1}^{N} (K_{ij} + \Delta_{ij})(u_{jn} - v_{jn}) = \omega_n (u_{in} + v_{in}) \tag{46}$$

and

$$\sum_{j=1}^{N} (K_{ij} - \Delta_{ij})(u_{jn} + v_{jn}) = \omega_n (u_{in} - v_{in}). \tag{47}$$

Multiplying these equations by $K-\Delta$ and $K+\Delta$, we find the following eigenvalue equations after a simple manipulation:

$$\sum_{j=1}^{N} [(K-\Delta)(K+\Delta)]_{ij} (u_{jn} - v_{jn}) = \omega_n^2 (u_{in} - v_{in}) \tag{48}$$

and

$$\sum_{j=1}^{N} [(K+\Delta)(K-\Delta)]_{ij} (u_{jn} + v_{jn}) = \omega_n^2 (u_{in} + v_{in}). \tag{49}$$

Although these equations are in principle decoupled, for the purpose of finding the local magnetization they are not so, since we are interested in finding mainly v (and not $u+v$ or $u-v$ alone). We will come back to this point later. Equations (48) and (49) can also be presented in more revealing form, namely (here we will drop indices to shorten the notation),

$$(K^2 - \Delta^2 \pm [\Delta, K])\phi^{(\pm)} = \lambda\, \phi^{(\pm)}, \tag{50}$$

where $\phi^{(\pm)} = u \pm v$ and $\lambda = \omega^2$. At this point it is interesting to notice that the nonzero commutator is the cause of non-Hermiticity in the eigenvalue problem. Had it been zero, the problem would be become real and symmetric. In fact, it is not difficult to show that

$$[\Delta, K]_{ij} = \Delta_{ij}(K_{ii} - K_{jj}). \tag{51}$$

Thus, it is only when all sites have the same number or nearest neighbors, i.e., when no dilution is present, that the problem becomes real and symmetric (and can therefore be solved analytically by a Fourier transform). Dilution always makes the eigenproblem non-Hermitian, although with real eigenvalues [even if we did not know the origin of Eq. (50), it would be easy to prove that all eigenvalues $\lambda \geqslant 0$].

Let us call $M^{(\pm)} = K^2 - \Delta^2 \pm [\Delta, K]$. An important feature of these matrices is that the left eigenvector $\phi^{(\pm)}$ of $M^{(\pm)}$ is the right eigenvector of $M^{(\mp)}$. Thus, if we use an algorithm that is capable of finding both the right and left eigenvectors of a non-Hermitian matrix, we only need to solve the problem for $M^{(+)}$, for instance. In this case, we may say that the $2N \times 2N$ problem has really been reduced to $N\times N$.

In terms of the eigenvectors $\phi^{(\pm)}$, the orthogonality relations of Eqs. (28) and (29) now read

$$\sum_{i=1}^{N} [\phi_{in}^{(+)*}\phi_{im}^{(-)} + \phi_{in}^{(-)*}\phi_{im}^{(+)}] = 2\ \delta_{nm} \tag{52}$$

and

$$\sum_{i=1}^{N} [\phi_{in}^{(-)*}\phi_{im}^{(+)} - \phi_{in}^{(+)*}\phi_{im}^{(-)}] = 0, \tag{53}$$

respectively. Moreover, using these relations and the definition of $\phi^{(\pm)}$, it is straightforward to show that the average site magnetization can be written as

$$\delta m_z = \frac{1}{4N}\sum_{n=2}^{N}\sum_{i=1}^{N} [|\phi_{in}^{(+)}|^2 + |\phi_{in}^{(-)}|^2] - \frac{1}{2}. \tag{54}$$

One issue that appears when diagonalizing the problem through solving Eq. (50) is that each eigenstate λ_n may have an eigenvector corresponding to any linear combination of the u_n and v_n vectors, and not just that $u_n \pm v_n$ (that is because each λ_n corresponds to at least two eigenfrequencies, namely $\pm\omega$, with $\omega_n = \sqrt{\lambda_n}$). Provided that there are no other degeneracies, one can sort out which combination is generated by noticing the following. Suppose that

$$\phi^{(+)} = c_+(u - v) \quad \text{and} \quad \phi^{(-)} = c_-(u + v), \tag{55}$$

then, it is easy to see that the normalization conditions for both $\phi^{(\pm)}$ and u, v imply $c_+c_- = 1$. We can then use Eqs. (46) and (47) to find that

$$(K - \Delta)\phi^{(+)} = \frac{\omega}{c_+^2}\phi^{(-)} \tag{56}$$

and

$$(K + \Delta)\phi^{(-)} = c_+^2\ \omega\ \phi^{(+)}. \tag{57}$$

These equations provide a way of determining the coefficient c_+ (and thus the actual mixing of degenerate eigenvectors). For instance, for a given eigenstate,

$$c_+^2 = \frac{1}{\sqrt{\lambda}} \frac{\sum_{i,j=1}^{N} \phi_i^{(+)}(K + \Delta)_{ij}\phi_j^{(-)}}{\sum_{i=1} \phi_i^{(+)}\phi_i^{(-)}}. \tag{58}$$

Once the c_+ coefficient has been determined, it is straightforward to determine the u_n and v_n vectors corresponding to a given (positive), nondegenerate eigenfrequency ω_n in a unique way. If additional degeneracy occurs, then one needs to introduce more coefficients (and consider combinations of all degenerate eigenvectors) in Eq. (55).

III. NUMERICAL SOLUTION OF THE NON-HERMITIAN EIGENPROBLEM

The numerical solution of the eigenproblem represented by Eq. (50) requires the full diagonalization of at least one real nonsymmetric matrix. However, before that, we need to generate the random dilution on a square lattice and set the appropriate boundary conditions. Another important point is that we can simplify the diagonalization by breaking the matrix into diagonal blocks, each one related to a single disconnected cluster. The diagonalizations can then be carried out separately on each block (for each disconnected cluster). Thus, the first task is to reorganize the matrices K and Δ following a hierarchy of disconnected cluster sizes. That involves only searching and sorting sites on the lattice (without any arithmetic or algebraic manipulation). Moreover, since we are interested only in what happens within the largest connected cluster (the only one relevant in the thermodynamic limit and below the percolation threshold),[7] we can concentrate our numerical effort into the diagonalization of the matrix block corresponding to that cluster alone.

The first step is to create a square lattice of size $N = L \times L$ (L being the lateral size of the lattice) with periodic boundary conditions in both directions. In order to have $N_A = N_B$, we choose L to be an even number. We fix the number of holes as the integer part of $(1-p)N$ and randomly distribute them over the lattice with uniform probability.

The second step is to identify all connected clusters that exist in the lattice for a given realization of dilution. Since most lattices we work with are quite dense (relatively few holes), we begin by finding all sites that belong to the cluster whose sites are nearest to one of the corners of the lattice. Once all sites in that cluster are found, they are subtracted from the lattice and the search begins again for another cluster. The process stops when all sites have been visited and the whole lattice is empty. The process of identifying sites for a particular cluster is the following. Starting from a fixed site i (the cluster seed), we check whether its four neighbors are occupied or empty. The occupied ones get the same tag number as the first site visited. Then we move on to the next side, $i+1$, and repeat the procedure. We continue until we reach the Nth site.

Along with identifying all sites belonging to each cluster, we also count then. That allows us to identify immediately the largest connected cluster in the lattice, whose number of sites we call N_c. We set a conversion table where the sequential number identifying a site in the largest cluster is associated to its coordinate in the original lattice. That allows us to later retrace the components of the eigenvectors of this cluster to their locations in the $L \times L$ lattice.

The process of identifying clusters is carried out under hard wall boundary conditions. In fact, it is only after the largest cluster is found that we force periodic boundary conditions. This is the third step. For that purpose, we sweep the bottom and top rows, as well as the right and left columns of the square lattice, and check whether these sites are neighbors of sites belonging to the largest cluster once periodic boundary conditions are assumed. It turns out that it is easier and faster to do that than to search and classify clusters directly from a lattice with periodic boundary conditions.

The fourth step consists of storing the information necessary to assemble the non-Hermitian matrices of the type shown in Eq. (36) for the largest cluster only. The algorithm is quite fast and allows one to generate and find the largest connected cluster in lattices as large as $L = 100$ in less than a second.

The information generated in the process of identifying the largest cluster and its structure is fed into a second rou-

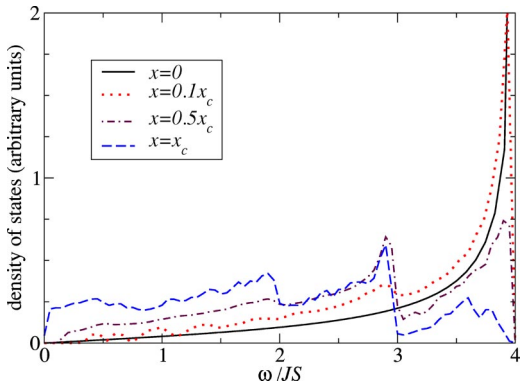

FIG. 1. Average density of states as a function of energy for four different site dilution fractions: $x=0$ (solid line), $x=0.1\ x_c$ (dotted line), $x=0.5\ x_c$ (dotted-dashed line), and $x=x_c$ (dashed line). Notice the two structures just below $\omega/JS=2$ and 3. The latter is already visible at $x=0.1\ x_c$, while the former becomes prominent only for $x\gtrsim 0.4\ x_c$. The data was obtained from 500 to 1000 realizations of a 36×36 lattice.

tine. There, one assembles both the non-Hermitian matrices of Eqs. (36) and (50). We have checked that the solution of both the $2N_c\times 2N_c$ and $N_c\times N_c$ problems provide identical solutions up to several digits for a particular realization of the dilution problem at various lattice sizes and dilution fractions. However, only the $N_c\times N_c$ problem was used to generate the data presented here.

It is important to point out that there exists an alternative formulation of the problem defined by Eq. (13), using generalized position and momentum operators (see Appendix A). In this formulation one can derive a sequence transformation that permits the calculation of eigenvalues and eigenvectors of the system Hamiltonian through the diagonalization of *Hermitian* matrices alone. However, from the computational point of view there is no substantial advantage of this approach with respect to the non-Hermitian one.

Since the solution of the non-Hermitian eigenvalue problem is less standard than the Hermitian case, we provide a description of the method in Appendix B.

IV. RESULTS

We have generated lattices with sizes ranging from $L=12$ to 36 and dilution fractions going from $x=0$ to x_c. The number of realizations for a given size and dilution fraction varied between 500 (nearly clean case) to 1000 (at the classical percolation threshold). The results of the numerical diagonalizations are described below.

A. Density of states

The ensemble averaged density of eigenstates as a function of frequency for $L=36$ is presented in Fig. 1 for several dilution fractions and compared to the well-known result for the clean case.[16] For a small dilution, there is little departure from the clean case, although a small structure is already visible at around $\omega/JS=3$. As the dilution increases, a peak and an edge develop at around this frequency. Notice that the

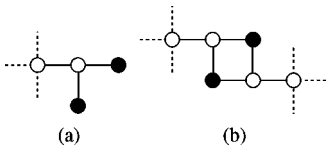

FIG. 2. The two dangling structures that occur in the $\omega/J=1$ (a) and 2 (b) eigenstates. The filled circles indicate $u_{in}\neq 0$, while the empty circles have $u_{in}=0$. All sites in these states have $v_{in}=0$, thus they do not contribute to the staggered magnetization.

overall trend is a decrease in the number of high-frequency modes, with the proportional increase in the number of low-frequency ones. Close to the percolation threshold, another structure appears at around $\omega/JS=2$. Thus, we see that the effect of dilution is to shift spectral weight from high to low frequencies in a nonuniform way. This tendency was also observed in Ref. 9 for small dilution.

Two additional very sharp peaks (not shown in Fig. 1) also exist in the density of states as the dilution increases. They occur at frequencies $\omega/JS=1,2$ and correspond to configurations where $v_{in}=0$ for all sites in the cluster, while $u_{in}=0$ for all but two sites. Their typical spatial structures are shown in Fig. 2. Since $v_{in}=0$ for all sites, these states do not contribute to the quantum corrections to the staggered magnetization.

For the clean case, it is simple to verify (based on the exact diagonalization of the problem) that the low frequency modes provide the largest contribution to δm_z. For the dilute lattice, the same is true, as can be seen in Fig. 3, where we have plotted

$$\delta m_z(\omega)=\frac{1}{N}\frac{\left\langle \sum_{i=1}^{N}\sum_{n=2}^{N}\delta m_i^z\ \delta(\omega-\omega_n)\right\rangle}{\left\langle \sum_{n=2}^{N}\delta(\omega-\omega_n)\right\rangle}. \tag{59}$$

As a result, we see that the transference of eigenmodes from high to low frequencies is the mechanism by which quantum fluctuations are enhanced as the dilution increases.

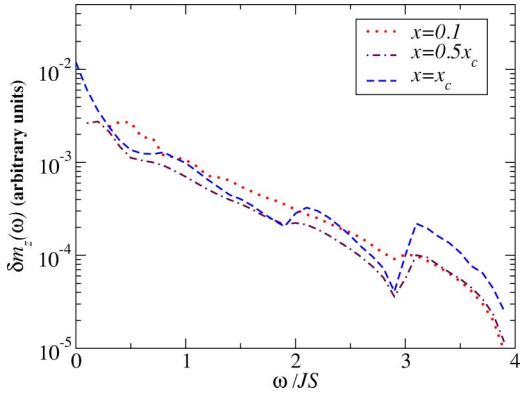

FIG. 3. Staggered magnetization per unit of magnetic site as a function of energy, $\delta m_z(\omega)$, under the same conditions of Fig. 1.

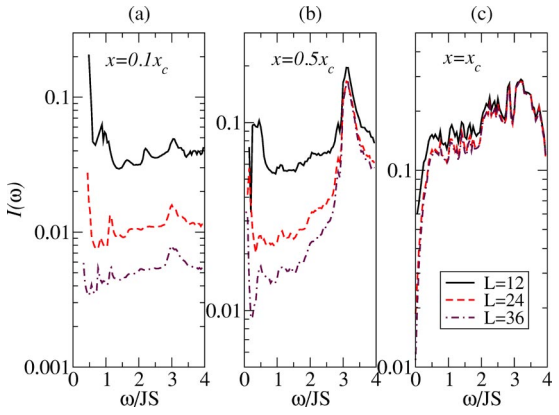

FIG. 4. Average inverse participation ratio, as defined in Eq. (60), as a function of energy for different lattice sizes and dilution fractions: (a) $x=0.1\,x_c$, (b) $x=0.5\,x_c$, and (c) $x=x_c$. As the dilution increases, states become more localized, beginning with those located in the high-energy part of the spectrum. Each curve shown corresponds to an average over 500 to 1000 realizations.

B. Inverse participation ratio

The nature of the eigenstates also changes as the dilution increases. The best way to characterize the nature of the states is through the return probability, that is, the probability that after some very long time a particle, moving in the percolating lattice, will return to its originating point. The return probability can be expressed in terms of the inverse participation ratio (IPR).[17] Here, we use a definition of the IPR involving the eigenvector component related to the quantum fluctuation corrections to the magnetization, namely,

$$I(\omega)=\frac{\sum_{n=2}^{N}\delta(\omega-\omega_n)I_n}{\sum_{n=2}^{N}\delta(\omega-\omega_n)}, \tag{60}$$

where

$$I_n=\frac{\sum_{i=1}^{N_c}v_{in}^4}{\left(\sum_{i=1}^{N_c}v_{in}^2\right)^2}. \tag{61}$$

In Fig. 4 we show the IPR as a function of energy for three lattice sizes. According to its definition, the IPR for extended states decreases as the system size increases, while for localized states the IPR is insensitive to any size variation. These trends are clearly visible in Fig. 4, namely, states are mostly extended when dilution is small and tend to localize as one gets closer to the percolation threshold. For intermediate dilution [Fig. 4(c)], we see that the states close to $\omega/JS=3$ are strongly localized while the remaining states are quite extended. As expected, the low frequency states tend to remain extended up to strong dilution.

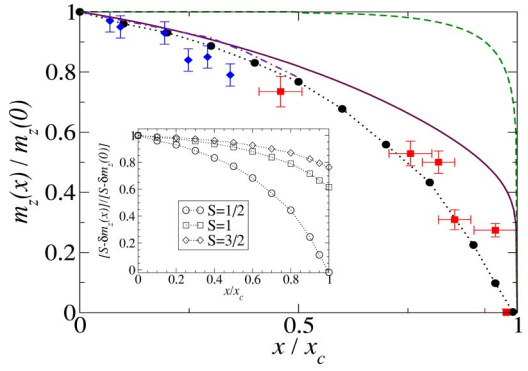

FIG. 5. The average staggered magnetization per unit of magnetic site. The results of the $S=1/2$ SWT simulations after finite-size scaling (circles) are compared with neutron scattering data (squares),[4] NQR data (diamonds),[19] and the fit to the QMC data from Ref. 8 (solid line). Also shown is the occupation fraction of the largest connected cluster N_c/N_m (dashed line) and the analytical result from the calculation of Ref. 9 (dashed-dotted line). Inset: the quantum fluctuation contribution to the staggered magnetization for different values of S.

C. Average magnetization

In the thermodynamic limit, the magnitude of the staggered magnetization per unit of lattice site m_z can be written as

$$m_z=\left(\frac{N_c}{N_m}\right)(S-\delta m_z), \tag{62}$$

where N_m is the total number of occupied sites in the lattice ($N_m=pN$). While the first factor on the right-hand side of Eq. (62) is purely classical, the second factor is purely quantum, namely, it measures how quantum fluctuations reduce magnetic order. Thus, since N_c vanishes at x_c, a quantum critical point below x_c can only exist if, for some $x^*<x_c$, we find $\delta m_z=S$. If, on the contrary, $\delta m_z<S$ at $x=x_c$, then the order is only lost at the percolation threshold and the transition is essentially classical. It is important to have in mind that the linear spin-wave approximation is well defined only when $\delta m_i^z \ll S$, for all $i=1,\ldots,N$. When $\delta m_i^z \approx S$ at a large number of sites, the approximation is not necessarily quantitatively correct.

Figure 5 shows the average staggered magnetization per unit of magnetic site as a function of dilution fraction, $m_z(x)$, when $S=1/2$. The points were obtained after finite-size scaling the ensemble averaged data taken from 12 different lattices sizes. As a consistency check, we have also calculated the staggered magnetization for the clean case ($x=0$, no ensemble average) with the same numerical procedure. We have found that $m_z(0)\approx 0.303$, consistent with values obtained by other methods.[18] Thus, at least at low dilution, the spin-wave approximation is quite accurate.

For comparison, we also show experimental data obtained for LCMO from both neutron scattering[4] and nuclear quadrupole resonance (NQR),[19] as well as the result of QMC simulations of the dilute Heisenberg AFM in a square lattice.[8] One can see that our simulations, based on the spin-wave approximation, capture the main features of the experi-

mental data, namely, a progressive decrease of the staggered magnetization up to the classical percolation threshold. At a dilution fraction very close to x_c, our simulations indicate that the staggered magnetization should vanish. The inset in Fig. 5 shows that the vanishing of the staggered magnetization occurs because δm_z goes to $1/2$ very close to the classical transition point. Thus, the same effect would not arise had we used $S>1/2$. The QMC simulations, on the other hand, predicts $\delta m_z<1/2$ at $x=x_c$, thus indicating that the transition is purely classical. The relatively small number of experimental points and the large error bars near the percolation threshold do not allow for an adequate distinction between a classical and a quantum transition for LCMO.

The discrepancy between our result and the QMC simulations for the staggered magnetization close to x_c should be seen as an indication that, while qualitatively correct, our approach fails quantitatively when the order parameter magnitude is significantly reduced locally. This is expected if we recall the assumption used in the derivation of Eq. (10). Nevertheless, the spin-wave approximation, having access to low-lying excited states and wave functions, allows us to understand in more detail, at least qualitatively, how the suppression of order due to quantum fluctuations takes place upon dilution. This is not the case for the QMC simulations. In fact, it is surprising that our calculations seem to agree with the experimental data better than the QMC. This can be understood by the fact that the experimental system may contain extra oxygen atoms that introduce holes in the CuO_2 planes, as well as next-nearest neighboring interactions that frustrate the AFM state and also introduce larger quantum fluctuations that are captured by the overestimation produced in the linear spin-wave theory. In fact, it is known that La_2CuO_4, has a nonzero frustrating next-nearest neighbor coupling.[4] That effectively decreases the spin per site to a value smaller than $1/2$, possibly bringing LCMO closer to a quantum critical point than the pure $S=1/2$ Heisenberg AFM.

D. Local fluctuations

We now turn to the question of local fluctuations. We have so far discussed the site-averaged demagnetization δm_z and used the criterion that it must be smaller than S for the order to persist. However, one could argue that some sites may have particularly large fluctuations; if these large fluctuations take place exactly at weak links of the largest connected cluster backbone, then they could be responsible for earlier destruction of the long-range order.[11] We have numerical evidence that this is unlikely, although the relatively small size of our lattices does not allow us to be conclusive. In Fig. 6 we show an intensity plot of the local quantum fluctuations δm_i in the largest connected cluster, very close to the percolation threshold, for a typical realization of a $L=32$. Notice that the largest fluctuations tend to appear only along dead-ends or dangling structures, and not in the links connecting blobs of the cluster backbone. The same trend is seen in all realizations that we have inspected.

E. Excited states

Equation (13) represents a system of N coupled harmonic oscillators with $A=K+\Delta$ and $B=K-\Delta$ being the spring constant and the inverse mass tensors, respectively (for an alternative description of the problem in terms of position and momentum operators, see Appendix A). For the simple model of elastic vibrations in a lattice, when $q_i=(a_i+a_i^\dagger)/\sqrt{2}$ has the meaning of a displacement of the ith atom around its equilibrium position, it is well known that the Hamiltonian of such a system can be mapped onto a problem of diffusion in a disordered lattice.[6] Analytical results for the related diffusive problem, as well as numerical simulations with large systems, allow one to understand several properties of the diluted vibrational model, such as the density of states (DOS) and the dynamical structure factor. Perhaps one of the most distinctive features is the existence of strongly localized excitations named fractons.[20] For dilution fractions $x<x_c$, these excitations appear in the high-frequency portion of the spectrum, beyond a certain crossover scale ω_c, while the low-frequency part is dominated by acoustic phonon like, nearly extended, excitations. At exactly $x=x_c$, the systems becomes a fractal and the fractons take over the entire spectrum.[6] Scaling considerations, as well as numerical simulations, have shown that, for a square lattice, the DOS behaves as

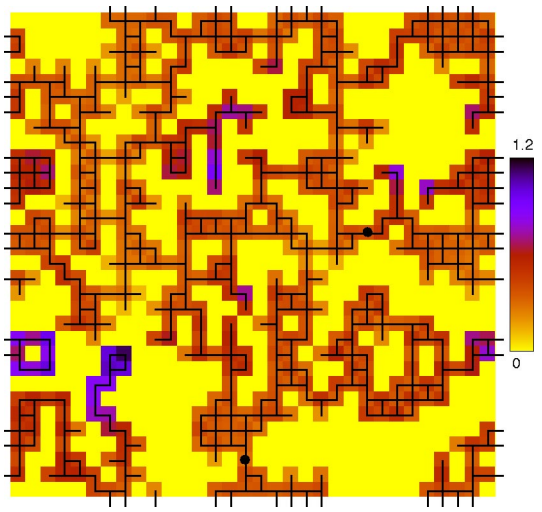

FIG. 6. The density plot of local demagnetization δm_i^z for a 32×32 lattice with periodic boundary conditions at $x\approx x_c$. Only sites belonging to the largest connected cluster are shown. The weak links present in the cluster are indicated by bullets.

$$\rho(\omega)\propto\begin{cases}\omega, & \omega<\omega_c\\ \omega^{1/3}, & \omega>\omega_c.\end{cases} \tag{63}$$

The crossover frequency depends critically on the dilution: $\omega_c\propto(x_c-x)^D$, where $D\approx91/48$. This is an important result because, for the elastic vibration problem, it is also possible to show that the quantum fluctuation corrections to the classical order parameter obey the relation

$$\delta m=\frac{1}{N}\sum_{n=1}^{N}\frac{1}{\omega_n}\overset{N\to\infty}{\to}\int_0^{\omega_{\max}}d\omega\frac{\rho(\omega)}{\omega}, \tag{64}$$

where $\{\omega_n\}$ are the nonzero eigenvalues of the corresponding Hamiltonian. Therefore, δm remains finite below and at the

percolation threshold, indicating that quantum fluctuations are likely not sufficiently enhanced by the dilution to destroy the existent long-range order.[10] We will get back to this point in Sec. V.

In order to investigate the existence of such fractons in the dilute 2D Heisenberg AFM, as well as to clarify the nature of its low-lying excitations, we have calculated the the dynamical structure factor,

$$S(\mathbf{q},\omega) = \int dt\, e^{-i\omega t} \sum_{i,j=1}^{N_m} e^{i\mathbf{q}\cdot(\mathbf{R}_i-\mathbf{R}_j)} \times \langle S_i^+(0)S_j^-(t) + S_i^-(0)S_j^+(t)\rangle. \tag{65}$$

By using Eqs. (3), (6), and (18), we can express $\mathcal{S}(\mathbf{q},\omega)$ in terms of Fourier transformations of the site-dependent Bogoliubov coefficients u_{in} and v_{in}. We find

$$\begin{aligned} S(\mathbf{q},\omega) = 2S \sum_{\omega_n\neq 0} \delta(\omega-\omega_n)[&\tilde{u}_n^{\mathcal{A}}(\mathbf{q})\tilde{u}_n^{\mathcal{A}}(-\mathbf{q}) + \tilde{v}_n^{\mathcal{A}}(\mathbf{q})\tilde{v}_n^{\mathcal{A}}(-\mathbf{q}) \\ &+ \tilde{u}_n^{\mathcal{A}}(\mathbf{q})\tilde{v}_n^{\mathcal{B}}(-\mathbf{q}) + \tilde{v}_n^{\mathcal{A}}(\mathbf{q})\tilde{u}_n^{\mathcal{B}}(-\mathbf{q}) + \tilde{u}_n^{\mathcal{B}}(\mathbf{q})\tilde{v}_n^{\mathcal{A}}(-\mathbf{q}) \\ &+ \tilde{v}_n^{\mathcal{B}}(\mathbf{q})\tilde{u}_n^{\mathcal{A}}(-\mathbf{q}) + \tilde{v}_n^{\mathcal{B}}(\mathbf{q})\tilde{v}_n^{\mathcal{B}}(-\mathbf{q}) + \tilde{u}_n^{\mathcal{B}}(\mathbf{q})\tilde{u}_n^{\mathcal{B}}(-\mathbf{q}) +], \end{aligned} \tag{66}$$

where the partial terms involving $\tilde{u}_n^{\mathcal{A},\mathcal{B}}$ are given by the Fourier transformation of u_n, namely,

$$\tilde{u}_n^{\mathcal{A},\mathcal{B}}(\mathbf{q}) = \sum_{i\in\mathcal{A},\mathcal{B}} u_{in}\, e^{i\mathbf{q}\cdot\mathbf{r}_i}, \tag{67}$$

and analogously for $\tilde{v}_n^{\mathcal{A},\mathcal{B}}$. Notice that the sum over sites runs only over one of the sublattices, $\mathcal{A}$ or $\mathcal{B}$, depending on the particular term. Thus, only four two-dimensional Fourier transformations are required in order to evaluate $\mathcal{S}(\mathbf{q},\omega)$.

We have computed numerically the Fourier transformations and calculated the average dynamical structure factor for lattices of size $L=32$ at several dilution fractions. Only sites within the largest connected cluster were taken into account. Averages were performed over 50 realizations for each case. The results are presented in the form of intensity plots in Fig. 7. To provide a better contrast, we have rescaled $\langle\mathcal{S}(\mathbf{q},\omega)\rangle$ by the function, $f(\omega)=\Sigma_q\langle\mathcal{S}(\mathbf{q},\omega)\rangle$. Only the data along two particular directions in momentum space are shown, namely $q=q_x=q_y$ and $q=q_x,q_y=0$, with $0\leqslant q\leqslant\pi$ (the lattice spacing is taken to be unit). For small dilution, the structure factor resembles closely that of the clean case, with some small broadening of the magnon branch due to the weak destruction of translation invariance. However, particularly along the $q_y=0$ direction, one can already notice a small hump at around $\omega/JS=3$, consistent with the peak-and-edge structure seen in Fig. 1. This feature becomes more prominent with increasing dilution. For dilution fractions larger than $0.6x_c$, another hump becomes visible at around $\omega/JS=2$, again consistent with the feature observed in Fig. 1 at the same frequency. Close to the percolation threshold, there exist three clear broad branches in the spectrum. While the dispersion of the high-frequency branch at $\omega/JS>3$ is hardly affected by the dilution, the opposite occurs with the low-frequency one, at $\omega/JS<2$, where the slope (magnon velocity) decreases with increasing dilution. We interpret the progressing breaking and bending of the magnon branch as the system becomes more diluted to the appearance of fractons. At $x=x_c$ the excitation spectrum has little resemblance to that of $x=0$ and even the long wavelength part is strongly modified. In between these two limits, there is a crossover from a magnon-dominated to a fracton-dominated spectrum. A three-branch structure for the spectral function in the spin-wave approximation was also found in Ref.9 However, the positioning of those branches and their relative intensity were different from what we observed in our numerical solution. We believe the cause of this discrepancy is the limited range of applicability of the perturbative treatment, which is expected to be accurate only in the weak dilution regime.

The gradual appearance, broadening, and motion of the branches are better represented in Fig. 8, where the rescaled average dynamical structure factor is shown as a function of frequency for a fixed momentum $q_x=0.4/\pi$ and $q_y=0$. The two-peak structure observed in our numerical data has some resemblance to the results of inelastic neutron scattering performed by Uemura and Birgeneau for the compound $Mn_xZn_{1-x}F_2$,[13] whose magnetic properties are described by the three-dimensional site-diluted random Heisenberg model with $S=5/2$. These authors observed two broad peaks which were associated with magnons (low-energy, extended) and fractons (high-energy, localized) excitations. The relative amplitude, width, and dispersion relations of these excitations were measured and were found consistent with the theoretical predictions by Orbach and Yu,[21] and Aharony and co-workers.[22] The scaling theory of the latter predicts that a two-peak spectrum appears at momenta $q\sim\xi^{-1}$, where ξ is the percolation correlation length (i.e., the typical linear size of the disconnected clusters when $x<x_c$). The relatively small size of the $L=32$ lattice does not allow us to make a similar quantitative comparison between these theories and our numerical results.

While we do observe a two-peak structure at sufficiently large dilution, we also see a third peak, although quite weak. This additional peak may be characteristic of square lattices; in the body-centered-cubic $Mn_xZn_{1-x}F_2$, there might exist a different multipeak structure. Moreover, th elarge broadening and limited energy resolution of the neutron-scattering experiments may have made such features unobservable in the data of Ref. 13. However, one aspect which seems different between the experimental data and our numerical simulations is the way the spectral weight is transferred between magnons and fractons as a function of dilution. While Uemura and Birgeneau see an increase (decrease) of high-frequency fractons (low-frequency magnons), we see the opposite: The low-frequency portion of the spectrum becomes more intense.

The averaging procedure recovers, to some extent, the translation invariance broken by the dilution. This allowed us to identify the large momentum part of the branches which, otherwise, would not be visible. However, the low momentum part is clearly visible even when no averaging is performed on the data (not shown). This fact, together with the strong dispersion of the lower energy branches, suggests that long wavelength propagating magnons are present for dilution fractions below the percolation threshold, and lose out to fractons at $x=x_c$. At $T=0$, these modes are responsible for the

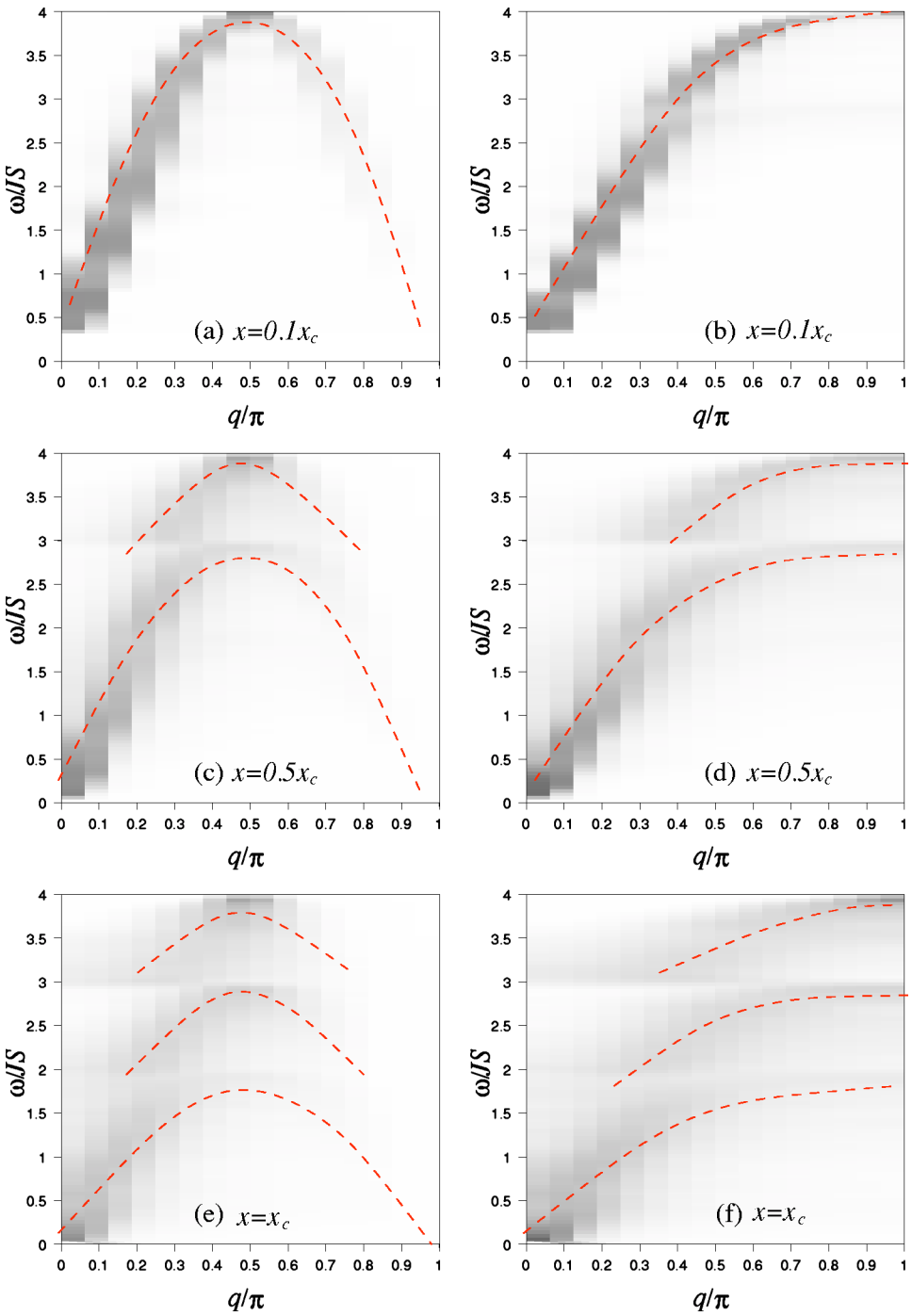

FIG. 7. Gray plots of the rescaled average dynamical structure factor sliced along two distinct directions in momentum space: $q_x=q_y=q$ [(a), (c), and (e)] and $q_x=q, q_y=0$ [(b), (d), and (f)]. Plots at different dilution fractions do not necessarily have the same arbitrary scale for the gray intensity. The most prominent branches are marked with dashed lines. Averaging for each plot was performed over 50 realizations of dilution.

quantum fluctuations that bring down the long range order. Their spectral weight becomes more important as the high-frequency states become more localized with increasing dilution. This feature is masked in Fig. 7 by the frequency-dependent rescaling, but is clear from Fig. 1. The high-frequency, high momentum modes are much less dispersive than the low-frequency, low momentum ones. In fact, particularly below $\omega/JS=3$, the magnon branch is q independent (i.e., broad in momentum) and thus strongly localized.

The low-frequency modes are likely not fully ballistic (coherent), given the large broadening seen in the structure factor, but should rather have a diffusive propagation at large scales. As to whether they remain two dimensional or gain a lower-dimensional character, our data is not conclusive.

V. UPPER BOUND FOR QUANTUM FLUCTUATIONS IN BOSONIC SYSTEMS

The possibility of a classification of quantum random systems into universality classes is an important theoretical problem with relevance to experiments. Random matrix classification schemes introduced by Wigner limited the classes of problems initially to the orthogonal, unitary, and symplectic classes,[23] but these were later extended to encompass the classes of chiral models[24] and models where the particle number is not a conserved quantity.[25] While most of the ran-

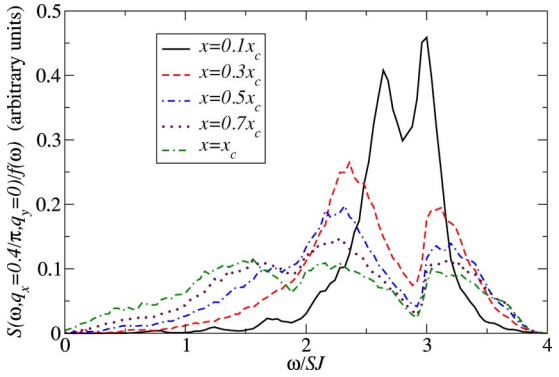

FIG. 8. Slice of the rescaled average dynamical structure factor for $q_x=0.4/pi$ and $q_y=0$ for $L=32$ and different dilution fractions.

dom matrix problems are related to fermionic spectra, there is renewed interest in the problem of bosonic random matrix theory.[26] Of particular importance is its application to the problem of diluted quantum magnets since these systems, in the limit of large spin S, can be approximately described, via linear spin-wave theory, as a problem of noninteracting bosons.[14]

One of the main differences between fermions and bosons is that, in addition to the symmetries of the underlying Hamiltonian, one must ensure that the bosonic spectrum is semipositive definite; this stability condition is not an issue in fermionic systems. However, it is automatically satisfied when the disorder is caused by site dilution.

Let us concentrate our discussion on systems whose Hamiltonian can be mapped onto a set of N coupled harmonic oscillators of the following kind:

$$H=\frac{1}{2}\sum_{i,j=1}^{N}(q_i\,A_{ij}\,q_j+p_i\,B_{ij}\,p_j). \tag{68}$$

Here, N is the total number of sites of the square lattice, while q_i and p_i represent generalized position and momentum operators at a lattice site i, respectively, such that $[q_i,p_j]=i\,\delta_{ij}$, with $i,j=1,\ldots,N$. The $N\times N$ matrices A and B are real, symmetric, and semipositive; in the most general case, they do not commute. The magnitude of quantum fluctuations are characterized by the mean-square deviation of the average value of these operators in the ground state: $\overline{q^2}=\Sigma_i\,\langle q_i^2\rangle/N$ and $\overline{p^2}=\Sigma_i\,\langle p_i^2\rangle/N$. As mentioned in Sec. IV C, if quantum fluctuations are unbounded at the percolating regime, then these mean values diverge and LRO is not possible, implying that order has to be destroyed before x_c is reached; that is, a quantum critical point should exist before the percolation threshold. Here we show that this is not the case and that LRO can persist up to and including x_c. As for the spin Hamiltonians approximated by Eq. (68), the exact disappearance of magnetic LRO may also depend on the spin value.

The eigenfrequencies of the harmonic oscillators of Eq. (68) can be shown to be those of

$$\Omega_L^2=AB \quad \text{or} \quad \Omega_R^2=BA. \tag{69}$$

Since, in general, $[A,B]$ is nonzero, the matrices Ω_L^2 and Ω_R^2 are non-Hermitian and distinct. However, it is simple to show that they have exactly the same real eigenvalues, ω_n^2, for $n=1,\ldots,N$. This is also true for the matrices $\Omega_C^2=B^{1/2}AB^{1/2}$ and $\tilde{\Omega}_C^2=A^{1/2}BA^{1/2}$. Therefore, the fluctuations of the position and momentum, averaged over all sites, can be written as[27]

$$\overline{q^2}=\frac{1}{2N}\mathrm{tr}(B\;{\Omega_C}^{-1})\leqslant\frac{b_*}{2}\kappa, \tag{70}$$

$$\overline{p^2}=\frac{1}{2N}\mathrm{tr}(A\;\tilde{\Omega}_C^{-1})\leqslant\frac{a_*}{2}\kappa, \tag{71}$$

where a_* and b_* denote the maximum eigenvalues of the semipositive definite matrices A and B, respectively, and we used that

$$\kappa=\frac{1}{N}\mathrm{tr}\;\Omega_C^{-1}=\frac{1}{N}\mathrm{tr}\;\tilde{\Omega}_C^{-1}=\int_0^{\omega_{\max}}d\omega\;\rho(\omega)\omega^{-1}, \tag{72}$$

since Ω_C and $\tilde{\Omega}_C$ share the same eigenvalues ($\omega_{\max}$ being the largest), with spectral density $\rho(\omega)$. Thus, the finiteness of the quantum fluctuations reduces to the problem of the convergence of the integral in Eq. (72) (quantum mechanics requires that $\overline{q^2}\;\overline{p^2}\geqslant 1/4$). Notice that the quantum fluctuation correction to the order parameter per unit of lattice site can be written as

$$\delta m_z=\alpha\;\overline{q^2}+\beta\;\overline{p^2}+\gamma, \tag{73}$$

where α, β, and γ are constants that depend on the particular model and order parameter under consideration.

We now turn to applying these general results to specific bosonic models based on Heisenberg Hamiltonians.

A. O(2) model

This model is realized, for example, in an array of Josephson junctions, where the variables q_i correspond to the linearized phase of the superconductor order parameter.[10,11] The matrices in Eq. (68) take the simple forms $A_{ij}=K_{ij}-\Delta_{ij}$ and $B_{ij}=(U/J)\delta_{ij}$, where $\Delta_{ij}=1(0)$ when the nearest-neighboring sites i,j are both occupied (otherwise) and $K_{ij}=\delta_{ij}\,\Sigma_{l=1}^{N}\Delta_{il}$, i.e., K_{ii} counts the number of nearest neighbors of site i. Here, J denotes the Josephson coupling and U is the island charging energy (usually, $J\gg U$). The same structure occurs in the case of vibrations in a diluted lattice.[6] For the O(2) model, the frequency eigenvalues are obtained from $\Omega^2=(U/J)A$. The problem of determining the density of states of the connectivity matrix A can be mapped onto a problem of diffusion in a disordered lattice.[6] It can be shown that the density of states of Ω goes $\rho(\omega)\propto\omega^{d^*-1}$. Up to the percolation threshold, $d^*=d=2$, while $d^*=\tilde{d}\approx 4/3$ exactly at $x=x_c$. Therefore, the site-averaged fluctuations are bounded, and the linear approximation (as well as order) is maintained as long the ratio J/U is large enough.

B. Heisenberg antiferromagnetic model

When we take $J_x=J_y=J_z$, the matrices take the form $A_{ij}=K_{ij}-\Delta_{ij}$ and $B_{ij}=K_{ij}+\Delta_{ij}$. It is useful to define a matrix $\Lambda=\Lambda^{\mathrm{T}}$ that has the effect of changing the signs of q_i and p_i for all sites i in one of the two sublattices. Thus, $B=\Lambda A\Lambda$, and $\Omega_R^2=\Lambda A\Lambda A$. Notice that $\Gamma=\Lambda A$, is not semipositive definite (in fact it is non-Hermitian), but has real eigenvalues with the same magnitude as those of Ω.

In the O(2) model, because $\Omega^2\propto A$, one can directly relate the energy eigenvalues of Ω to those of the matrix A. In the AFM case, we need to obtain the density of states of $\Gamma=\Lambda A$, which is not simply related to that of A (since $[\Lambda,A]\neq 0$ in general for diluted systems). This nontrivial relation between the eigenvalues of Ω and A is generally present in bosonic problems. For example, a similar problem also appears in the work of Gurarie and Chalker in the relation between their stiffness and frequency eigenvalues.[26]

The problem of determining the density of states of Γ for a random dilution problem is one of the interesting open questions related to the important difference between random fermionic and bosonic systems. In a fermionic problem this question would be already answered by matching the symmetries of Γ to the Cartan classification table.[25] However, one cannot substitute the matrix A by an arbitrary random matrix with similar symmetries, that would violate the semipositive definite constraint. In this work we do not attempt to analytically resolve this problem; however, we find numerical evidence that the density of states of Γ^2 follows that of A at low energies.

Our simulations show that the site-averaged fluctuations δm_i^z are bounded, both below and at the percolation threshold. This means that order should exist up to and including the critical dilution x_c, as long as δm_i is small compared to the value of the spin S. Recalling Eq. (62), we conclude that there could be a minimum value $S_{\min}$ for the spin, below which there is a quantum phase transition for dilutions $x<x_c$. An effective local spin smaller than $1/2$ can be realized in a bilayer system with antiferromagnetic interlayer coupling.[28]

C. XXZ model

In this case, $J_x=J_y\neq J_z$. We then have $A_{ij}=K_{ij}-\Delta_{ij}$ and $B_{ij}=K_{ij}-\gamma\Delta_{ij}$, where γ measures the anisotropy. Alternatively, we can write $B=(1+\gamma/2)A+(1-\gamma/2)\Lambda A\Lambda$, and so $\Omega^2=(1+\gamma/2)A^2+(1-\gamma/2)\Lambda A\Lambda A$ (notice that for $\gamma\to-1$ we have the same problem as the AFM). The analysis is similar to the previous two cases. The amount of fluctuations is controlled by the anisotropy, and it can be shown to be bounded if the density of states follows that of the AFM case.

VI. DISCUSSION AND CONCLUSIONS

In this work we have studied the role played by site dilution in enhancing quantum fluctuations in the ground state of the Heisenberg antiferromagnet in a square lattice. Using the linear spin-wave approximation for this model, we have performed exact numerical diagonalizations for lattices up to 36×36, with dilution fractions going from the clean limit to the classical percolation threshold. Our results indicate a progressive, nonuniform shift of spectral weight in the spin-wave excitation spectrum from high and to low frequency as the dilution increases, with the high-frequency part becoming more localized. The higher density of low-frequency, long wavelength excitations leads to strong quantum fluctuations and a decrease in the magnitude of the staggered magnetization. For dilutions very close to the classical percolation threshold, we have found that quantum fluctuations are sufficiently strong to nearly match the clean-limit magnitude of the magnetization when $S=1/2$, but not for higher spins. This is consistent with recent neutron-scattering experiments with the $S=1/2$ dilute Heisenberg antiferromagnet $La_2Cu_{1-x}(Zn,Mg)_xO_4$, which show that long-range order disappears at around the classical percolation threshold. However, quantum Monte Carlo simulations suggest that quantum fluctuations should remain small and that the destruction of long-range order is controlled only by the disappearance of the infinite connected cluster. We understand this discrepancy between the quantum Monte Carlo results and the linear spin-wave theory near the classical percolation threshold as an indication that the latter has its validity limited, as the magnitude of the order parameter is too small.

While perhaps not quantitatively accurate, our simulations do allow us to probe into nature of the low-lying excited states of the dilute antiferromagnet. We observe two clear humps in the density of states at frequencies $\omega/JS=2$ and 3. By calculating the ensemble-averaged dynamical structure factor, we were able to associate the appearance of these humps with the breaking of the clean-limit magnon branch into three distinct but broad branches. The new branches tend to be strongly localized (nondispersive) at high frequencies and have a diffusive, rather than ballistic, nature at low frequencies. In the literature, the multipeak structure had been associated with the appearance of fractons in the excitation spectrum as the dilution increases. From our simulations, it seems that the picture is somewhat more complex. Besides the overall broadening, the position of the high-frequency branch remains close to the corresponding portion of original clean-limit magnon branch, while the magnon velocity (the $d\omega/dq$ slope) in the low-frequency branch is continuously reduced with increasing dilution. Therefore, it appears that the fracton character also contaminates the low-frequency branch. However, the lack of resolution due to the finite size of our lattices does not allow for a conclusive picture. We did not attempt, however, to study fracton states which can possibly occur above the percolation threshold.[20,29]

It is important to remark that, in principle, due to Anderson localization in two dimensions, we expect that in the infinite system all excitations should in fact be localized for any finite dilution. In order to probe more carefully strong localization and the consequent exponential decay in real space, we need not only much larger lattices, but also to calculate two-point correlators, which goes beyond the applicability of linear spin-wave approximation. For that same reason, we were not able to evaluate quantities such as the spin stiffness, which involves matrix elements of higher than bilinear operators.

We also studied the question of local quantum fluctuations as a way to destroy long-range order. For finite-size lattices, we found that the weak links do not show strong quantum

renormalizations. That provides some indication that local quantum fluctuations may not be sufficient to change the dominance of the classical percolation picture.

Using a more general analytical formulation, we have argued that there exists an upper bound for the quantum fluctuations in any model with a classically ordered ground state whose Hamiltonians can be mapped onto that of a system of coupled harmonic oscillators. The amount of quantum fluctuations depends directly on the low-energy behavior of the density of states of the associated bosonic problems. Our exact diagonalization of the linear spin wave Hamiltonian on a percolating lattice led us to identify the value of the upper bound for one particular type of model and can readily be used to find similar values for any other bosonic model. This could be used to study a large class of spin Hamiltonians that can be bosonized in the ordered phase.

ACKNOWLEDGMENTS

We thank I. Affleck, H. Baranger, J. Chalker, A. Chernyshev, M. Greven, J. Moore, C. Mudry, A. Sandvik, T. Senthil, O. Sushkov, O. Vajk, A. Vishwanath, and M. Vojta for useful conversations. We acknowledge financial support from CNPq and PRONEX in Brazil (E.R.M.), and from the NSF through Grants No. DMR-0103003 (E.R.M.), No. DMR-0343790 (A.H.C.N.), and No. DMR-0305482 (C.C.).

APPENDIX A: FORMULATION IN TERMS OF COUPLED HARMONIC OSCILLATOR

The spin-wave Hamiltonian of Eq. (13) can be represented in terms of position and momentum operators. In this language, it becomes more transparent that the problem of finding the eigenvalues and eigenvectors of the Hamiltonian can be solved by the diagonalization of two real symmetric matrices, an alternative to the non-Hermitian eigenvalue formulation of Sec. II B.

Let us perform the following operator transformation:

$$q_i = \frac{a_i + a_i^\dagger}{\sqrt{2}} \quad \text{and} \quad p_i = \frac{a_i - a_i^\dagger}{i\sqrt{2}}, \tag{A1}$$

for all $i=1,\ldots,N$. Notice that the operators q_i and p_i obey the canonical position-momentum commutation relations. It is convenient to adopt a matrix formulation for the problem, namely,

$$H = \frac{JS}{2}(q^T \mathbf{A}\ q + p^T \mathbf{B}\ p), \tag{A2}$$

where $x=\{x_i\}_{i=1\ldots N}$ and $p=\{p_i\}_{i=1\ldots N}$ denote vectors of position and momentum operators, while $[\mathbf{A}]_{ij}=K_{ij}+\Delta_{ij}$, and $[\mathbf{B}]_{ij}=K_{ij}-\Delta_{ij}$. The quantum fluctuation correction to the sublattice magnetization can be written as

$$\delta m = \frac{1}{2N}\mathrm{tr}[\langle q\ q^T\rangle + \langle p\ p^T\rangle] - \frac{1}{2}. \tag{A3}$$

We can diagonalize $\mathbf{B}$ through an orthogonal transformation $\mathbf{U}$,

$$\mathbf{U}^T\mathbf{B}\mathbf{U} = \mathbf{b} \quad \text{(diagonal)} \tag{A4}$$

and define new coordinates such that

$$q = \mathbf{U}q' \quad \text{and} \quad p = \mathbf{U}\ p'. \tag{A5}$$

Defining $\mathbf{A}'=\mathbf{U}^T\mathbf{A}\ U$, we then have that

$$H = \frac{JS}{2}(q'^T\mathbf{A}'\ q' + p'^T\mathbf{b}\ p') \tag{A6}$$

and

$$\delta m = \frac{1}{2N}[\mathrm{tr}(\langle q'\ q'^T\rangle) + \mathrm{tr}(\langle p'\ p'^T\rangle)] - \frac{1}{2}. \tag{A7}$$

It is not difficult to prove that all elements in the diagonal of $\mathbf{b}$ are positive except one, b_1, which is zero. In order to eliminate this zero mode, we subtract the corresponding row or line in all vectors and matrices, which amounts to a reduction in the Hilbert space (or, alternatively, to set $q'_0=0$): $\{q'\}_N \to \{q'\}_{N-1}$ and $\{p'\}_N \to \{p'\}_{N-1}$. Also, $[\mathbf{A}']_{N\times N} \to [\mathbf{A}']_{N-1\times N-1}$ and $[\mathbf{b}]_{N\times N} \to [\mathbf{b}]_{N-1\times N-1}$. Notice that now all $b_k>0$, $k=2,\ldots N$. Thus, in this new space, we can perform the following rescaling:

$$q'' = \mathbf{b}^{-1/2}q' \quad \text{and} \quad p'' = \mathbf{b}^{1/2}p', \tag{A8}$$

which allows us to write

$$H = \frac{JS}{2}(q''^T\mathbf{A}''\ q'' + p''^T p''), \tag{A9}$$

with $\mathbf{A}''=\mathbf{b}^{1/2}\mathbf{A}'\mathbf{b}^{1/2}$ as well as

$$\delta m = \frac{1}{2N}[\mathrm{tr}(\mathbf{b}\langle q''q''^T\rangle) + \mathrm{tr}(\mathbf{b}^{-1}\langle p''\ p''^T\rangle) + \langle p'^2_1\rangle] - \frac{1}{2}, \tag{A10}$$

where the last term within the square brackets reflects the existence of a zero mode. It is useful now to return to the site basis by carrying out the inverse rotation,

$$q''' = \mathbf{U}q'' \quad \text{and} \quad p''' = \mathbf{U}\ p'', \tag{A11}$$

such that

$$H = \frac{JS}{2}(q'''^T\mathbf{C}\ q''' + p'''^T\ p'''), \tag{A12}$$

where $\mathbf{C}=\mathbf{U}\ \mathbf{A}''\ \mathbf{U}^T$ is the new connectivity matrix. If we define

$$\mathbf{B}^{1/2} = \mathbf{U}\ \mathbf{b}^{1/2}\ \mathbf{U}^T \quad \text{and} \quad \mathbf{B}^{-1/2} = \mathbf{U}\ \mathbf{b}^{-1/2}\ \mathbf{U}^T \tag{A13}$$

within the subspace $N-1\times N-1$ where no zero mode is present, we can write the connectivity matrix as

$$\mathbf{C} = \mathbf{B}^{1/2}\mathbf{A}\mathbf{B}^{1/2}. \tag{A14}$$

Also, notice that the inverse rotation does not change the expression of the sublattice magnetization,

$$\delta m = \frac{1}{2N}[\mathrm{tr}(\mathbf{b}^{-1}\langle q'''q'''^T\rangle) + \mathrm{tr}(\mathbf{b}\langle p'''p'''^T\rangle) + \langle p'^2_0\rangle] - \frac{1}{2}. \tag{A15}$$

We can now perform the last operation, namely, the diagonalization of the connectivity matrix,

$$q^{iv} = \mathbf{V} q''' \quad \text{and} \quad p^{iv} = \mathbf{V}\, p''', \tag{A16}$$

yielding

$$H = \frac{JS}{2}(q^{iv\ T}\mathbf{c}\ q^{iv} + p^{iv\ T} p^{iv}), \tag{A17}$$

where

$$\mathbf{V}^T\mathbf{C}\ \mathbf{V} = \mathbf{c} \quad \text{(diagonal)}, \tag{A18}$$

with all $c_n > 0$, $n = 1, \ldots N-1$. We finally arrive to a system of decoupled harmonic oscillators. The quantum fluctuation part of the magnetization becomes

$$\delta m = \frac{1}{2N}[\mathrm{tr}(\mathbf{b}^{-1}\mathbf{V}^T\langle q^{iv} q^{iv\ T}\rangle\mathbf{V}) + \mathrm{tr}(\mathbf{b}\ \mathbf{V}^T\langle p^{iv} p^{iv\ T}\rangle\mathbf{V}) + \langle p'^2_0\rangle] - \frac{1}{2}. \tag{A19}$$

However, we know that

$$[\langle q^{iv} q^{iv\ T}\rangle]_{nm} = \delta_{nm}\,\langle q_n^{iv\ 2}\rangle = \frac{1}{2}[\mathbf{c}]^{-1/2}_{nm} \tag{A20}$$

and

$$[\langle p^{iv}\ p^{iv\ T}\rangle]_{nm} = \delta_{nm}\langle p_n^{iv\ 2}\rangle = \frac{1}{2}[\mathbf{c}]^{1/2}_{nm}. \tag{A21}$$

Therefore,

$$\delta m = \frac{1}{4N}[\mathrm{tr}(\mathbf{b}^{-1}\ \mathbf{V}^T\ \mathbf{c}^{-1/2}\ \mathbf{V}) + \mathrm{tr}(\mathbf{b}\ \mathbf{V}^T\ \mathbf{c}^{1/2}\ \mathbf{V}) + \langle p'_0{}^2\rangle] - \frac{1}{2}. \tag{A22}$$

It is interesting to notice that, since $\mathbf{A} = \mathbf{O}\ \mathbf{B}\ \mathbf{O}$, we have that

$$\mathbf{C} = \Omega^2, \tag{A23}$$

where

$$\Omega = \mathbf{B}^{1/2}\ \mathbf{O}\ \mathbf{B}^{1/2}. \tag{A24}$$

Thus, it is easy to see that if $\mathbf{C}$ were a positive matrix, then we would be able to write $\mathbf{V}^T\mathbf{c}^{1/2}\mathbf{V} \equiv \mathbf{C}^{1/2} = \Omega$. That would allow us to simplify the expression for the sublattice magnetization a step further. However, the connectivity matrix is not necessarily positive.

APPENDIX B: NUMERICAL DIAGONALIZATION OF THE NON-HERMITIAN MATRIX

The diagonalization of the non-Hermitian matrices consists of five steps. First, the real (but asymmetric) matrix $M^{(+)}$ is reduced to an upper Hessenberg form through an orthogonal transformation, namely, $A = QM^{(+)}Q^T$. This is done by using the LAPACK subroutines DGEHRD and DORGHR. Second, we use the LAPACK subroutine DHSEQR to perform the Schur factorization of the Hessenberg matrix: $A = ZTZ^T$. That allows us to obtain the eigenvalues and the Schur vectors, which are contained in the orthogonal matrix Z. Third, using another LAPACK subroutine, DTREVC, we extract from Z both right and left eigenvectors of $M^{(+)}$. In the fourth step we renormalize all eigenvectors $\{\phi^{(\pm)}\}$ such that they satisfy Eq. (52) [the condition in Eq. (53) is automatically satisfied], sort the eigenvalues $\{\lambda_n\}$ in ascending order, and extract the zero mode from the spectrum. For some realizations, the lowest eigenvalues next to the zero mode cannot be distinguished from the zero mode itself and are therefore neglected. Finally, the correct linear combination of $\phi_n^{(\pm)}$ that provides the correct u_n and v_n for each positive eigenfrequency $\omega_n = \sqrt{\lambda_n}$ is obtained according to the algorithm presented in Sec. II D.

[1] E. Abrahams, S. V. Kravchenko, and M. P. Sarachik, Rev. Mod. Phys. **73**, 251 (2001).

[2] P. J. Hirschfeld and W. A. Atkinson, J. Low Temp. Phys. **126**, 881 (2002).

[3] G. R. Stewart, Rev. Mod. Phys. **73**, 797 (2001).

[4] O. P. Vajk, P. K. Mang, M. Greven, P. M. Gehring, and J. W. Lynn, Science **295**, 1691 (2002); O. P. Vajk, M. Greven, P. K. Mang, and J. W. Lynn, Solid State Commun. **126**, 93 (2003).

[5] M. E. J. Newman and R. M. Ziff, Phys. Rev. Lett. **85**, 4104 (2000).

[6] T. Nakayama, K. Yakubo, and R. L. Orbach, Rev. Mod. Phys. **66**, 381 (1994).

[7] D. Stauffer and A. Aharony, *Introduction to Percolation Theory*, 2nd ed. (Taylor and Francis, London, 1994).

[8] A. W. Sandvik, Phys. Rev. B **66**, 024418 (2002).

[9] A. L. Chernyshev, Y.-C. Chen, and A. H. Castro Neto, Phys. Rev. B **65**, 104407 (2002).

[10] This problem was studied recently by A. Vishwanath and T. Senthil (unpublished).

[11] N. Bray-Ali and J. E. Moore, cond-mat/0305009.

[12] T. Terao, K. Yakubo, and T. Nakayama, Phys. Rev. B **49**, 12281 (1994).

[13] Y. J. Uemura and R. J. Birgeneau, Phys. Rev. B **36**, 7024 (1987).

[14] T. Holstein and H. Primakoff, Phys. Rev. **58**, 1098 (1940).

[15] For a more thorough discussion of the non-Hermitian eigenvalue problem that results from Bogoliubov transformations in bosonic systems, see J.-P. Blaizot and G. Ripka, *Quantum Theory of Finite Systems* (MIT Press, Cambridge, MA, 1986).

[16] A. Auerbach, *Interacting Electrons and Quantum Magnetism* (Springer, New York, 1994).

[17] F. Wegner, Z. Phys. B **36**, 209 (1980).

[18] J. D. Reger and A. P. Young, Phys. Rev. B **37**, 5978 (1988); R. R. P. Singh, *ibid.* **39**, 9760 (1989); N. Trivedi and D. M. Ceperley, *ibid.* **40**, 2737 (1989); G. E. Castilla and S. Chakravarty, *ibid.* **43**, 13687 (1991); J.-I. Igarashi, *ibid.* **46**, 10763 (1992).

[19] M. Corti, A. Rigamonti, F. Tabak, P. Carreta, F. Licci, and L. Raffo, Phys. Rev. B **52**, 4226 (1995).
[20] S. Alexander and R. Orbach, J. Phys. (France) Lett. **43**, L625 (1982).
[21] R. Orbach and K. W. Yu, J. Appl. Phys. **61**, 3689 (1987).
[22] A. Aharony, S. Alexander, O. Entin-Wohlman, and R. Orbach, Phys. Rev. B **31**, 2565 (1985); Phys. Rev. Lett. **58**, 132 (1987).
[23] E. P. Wigner, Proc. Cambridge Philos. Soc. **47**, 790 (1951); Ann. Math. **67**, 325 (1958).
[24] R. Gade, Nucl. Phys. B **398**, 499 (1993).
[25] A. Altland and M. R. Zirnbauer, Phys. Rev. B **55**, 1142 (1997).
[26] V. Gurarie and J. T. Chalker, Phys. Rev. Lett. **89**, 136801 (2002); Phys. Rev. B **68**, 134207 (2003).
[27] When defining the inverse matrices in Eqs. (70) and (71), the subspaces corresponding to zero eigenvalue states have been eliminated.
[28] A. W. Sandvik, Phys. Rev. Lett. **89**, 177201 (2002); O. P. Vajk and M. Greven, *ibid.* **89**, 177202 (2002).
[29] G. Polatsek, O. Entin-Wohlman, and R. Orbach, Phys. Rev. B **39**, 9353 (1989).